Dalton Transactions

ROYAL SOCIETY OF CHEMISTRY

PAPER

View Article Online
View Journal | View Issue

Cite this: *Dalton Trans.*, 2025, **54**, 616

Investigating the formation of metal nitride complexes employing a tetradentate bis-carbene bis-phenolate ligand†

Romain Kunert,[a,b] Diego Martelino,[a] Samyadeb Mahato,[a] Nicholas M. Hein,[a] Jason Pulfer,[a] Christian Philouze,[b] Olivier Jarjayes, *[b] Fabrice Thomas *[b] and Tim Storr *[a]

The synthesis of Mn^{V} and Cr^{V} nitride complexes of a pro-radical tetradentate bis-phenol bis-N-heterocyclic carbene ligand $\mathbf{H_2L^{C2O2}}$ was investigated. Employing either azide photolysis of the Mn^{III} precursor complex $\mathbf{MnL^{C2O2}(N_3)}$ or a nitride exchange reaction between $\mathbf{MnL^{C2O2}(Br)}$ and the nitride exchange reagent **Mnsalen(N)** failed to provide a useful route to the target nitride $\mathbf{MnL^{C2O2}(N)}$. Experimental results support initial formation of the target nitride $\mathbf{MnL^{C2O2}(N)}$, however, the nitride rapidly inserts into a Mn–C_{NHC} bond. A second insertion reaction results in the isolation of the doubly inserted ligand product $\mathbf{[H_2L^{C2O2}(N)]^+}$ in good yield. In contrast, the Cr analogue $\mathbf{CrL^{C2O2}(N)}$ was readily prepared and characterized by a number of experimental methods, including X-ray crystallography. Theoretical calculations predict a lower transition state energy for nitride insertion into the M–C_{NHC} bond for Mn in comparison to Cr, and in addition the N-inserted product is stabilized for Mn while destabilized for Cr. Natural bond order (NBO) analysis predicts that the major bonding interaction (π M≡N → σ^* M–C_{NHC}) promotes nucleophilic attack of the nitride on the carbene as the major reaction pathway. Finally, one-electron oxidation of $\mathbf{CrL^{C2O2}(N)}$ affords a relatively stable cation that is characterized by experimental and theoretical analysis to be a metal-oxidized d^0 Cr^{VI} species.

Received 17th June 2024,
Accepted 1st November 2024

DOI: 10.1039/d4dt01765j

rsc.li/dalton

1. Introduction

High valent metal nitrido (N^{3-}) species are of significant interest as proposed intermediates in biological and industrial processes,[1–3] as well as N-atom transfer chemistry.[4–13] A number of bioinspired Fe nitride complexes have been studied in the context of nitrogen fixation,[14–20] and recent advances understanding synthetic FeS clusters have provided important information on the identity of activated Fe–N species.[21–25] The stability and reactivity of discrete transition metal nitrides depends on factors such as metal identity and oxidation state, ligand identity, and overall geometry.[26–28] Early transition metal nitrides are generally stabilized,[29,30] and exhibit nucleophilic reactivity from either filled M≡N π orbitals or the nitride lone pair.[27,31–33] In contrast, late transition metal nitrides can be either isolated or described as transient intermediates, exhibiting electrophilic reactivity *via* M≡N π^* orbitals.[28,34–42] Interestingly, a number of metal nitride complexes display ambiphilic reactivity,[43–45] and subtle changes to the coordination environment can result in tunable reactivity at the nitride.[33,35,46–49]

We have reported that oxidation of nitrido metal salen complexes (see Scheme 1 for example salen $\mathbf{H_2Sal^R}$) results in an electronic structure that can be modulated *via* alteration of the electron-donating ability of *para*-R phenolate substituents, without changing the geometry at the metal center.[33,50–52] Salen ligands are redox-active and have been documented to undergo oxidation or reduction at the ligand in place of the metal.[53–56] In certain exceptional cases both metal and ligand oxidation can occur.[57–59] We, and others, have also reported that the formation of a Mn^{VI} salen nitride results in rapid homocoupling of the nitride to form N_2,[52,60,61] however formation of a ligand radical (employing strongly electron-donating *para*-R substituents such as R = NMe_2) precludes this homocoupling.[52] Recent work with Ru[62] and Mo[63,64] nitrides has explored the homocoupling pathway and documented the formation of μ-nitrido products. In addition to homocoupling, Mn salen nitrides have been investigated in the context of the hydrogen atom bond dissociation free energy of the associated

[a]*Department of Chemistry, Simon Fraser University, Burnaby, British Columbia, V5A 1S6, Canada. E-mail: tim_storr@sfu.ca*
[b]*Univ. Grenoble Alpes, CNRS, DCM, F-38000 Grenoble, France. E-mail: Olivier.Jarjayes@univ-grenoble-alpes.fr, Fabrice.Thomas@univ-grenoble-alpes.fr*

† Electronic supplementary information (ESI) available. CCDC 2359452, 2359453, 2359455 and 2359456. For ESI and crystallographic data in CIF or other electronic format see DOI: https://doi.org/10.1039/d4dt01765j

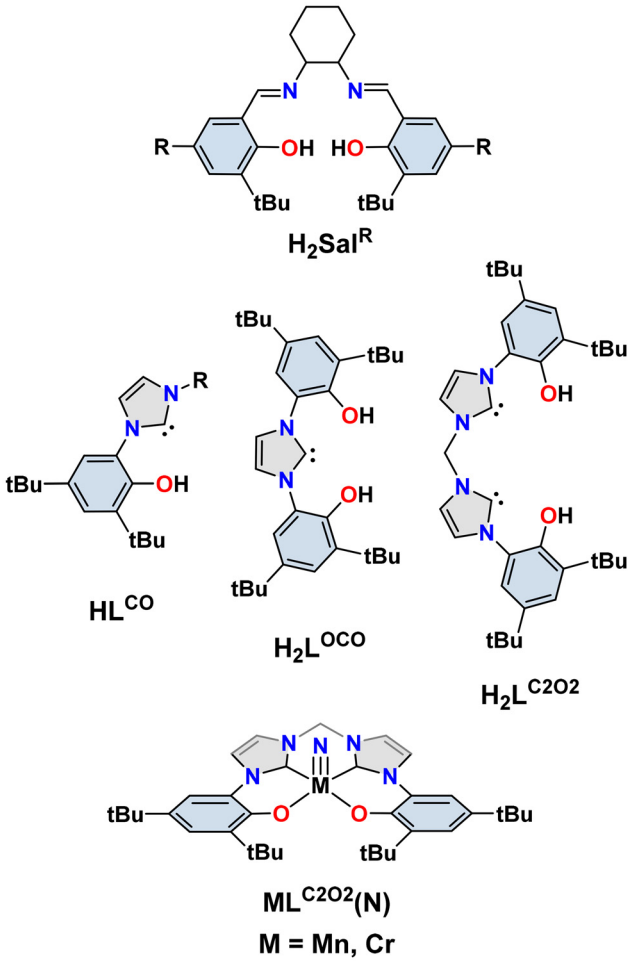

Scheme 1 Representative Salen (H_2Sal^R) and N-heterocyclic carbene arylphenoxide ligands (HL^{CO}, H_2L^{OCO}, H_2L^{C2O2}) and target metal nitride complexes of a tetradentate bis-carbene bis-phenolate ligand $ML^{C2O2}(N)$ M = Mn, Cr.

imido complexes,[65] generation of ammonia by proton-coupled electron transfer,[66–68] and as a catalyst for ammonia oxidation.[69]

In the current work we investigate the formation and stability of Mn and Cr nitride complexes using a tetradentate bis-phenol bis-N-heterocyclic carbene ligand $\mathbf{H_2L^{C2O2}}$,[70] and compare to our recently published work using salen ligands (Scheme 1).[33,50–52] The strong σ-donating capability (and potential for π-backbonding) of NHC ligands results in facile binding to electron-rich metals for catalytic applications.[71,72] A number of high oxidation state metal complexes employing NHC ligands have also been characterized, including those of V^{V},[73] Co^{IV},[38,74] Cu^{III},[75] Ni^{III},[70,76,77] $Mn^{IV/V}$,[78] $Fe^{IV–VII}$,[14,16,19,20] Mo^{VI},[79] and Nb^{V}.[80] Of particular relevance to the work herein is the use of tripodal carbene ligand frameworks by Smith and Meyer to stabilize high oxidation state Mn, Fe, and Co nitrides.[14,16,19,20,78] In certain cases the nitride ligand has been shown to insert into the M–C_{NHC} bond to form an imine.[16,20,38]

Redox-active NHC ligands have been described,[81–88] and the presence of arylphenoxide units results in a significant lowering of the oxidation potential of the ligand. Indeed, a series of Ni^{II} ligand radical complexes of the $\mathbf{HL^{CO}}$, $\mathbf{H_2L^{OCO}}$, and $\mathbf{H_2L^{C2O2}}$ (Scheme 1) ligands have been characterized in the solid state.[70,76,77] The different bonding properties of the imine and NHC donors in the salen and $\mathbf{H_2L^{C2O2}}$ ligands (Scheme 1) juxtaposed with the similar metal binding geometry and capacity for ligand-based oxidation presents an interesting opportunity to compare the formation and stability of the respective Cr and Mn nitride complexes.

2. Results and discussion

2.1. Synthesis of Mn precursors

Reaction of the bromide salt of the tetradentate bis-carbene bis-phenolate ligand $\mathbf{H_2L^{C2O2}}$**·2HBr** with $Mn(OAc)_2$ and NEt_3 in CH_3CN solvent afforded the Mn^{III} complex $\mathbf{MnL^{C2O2}(Br)}$ (Scheme 2). The synthesis of $\mathbf{MnL^{C2O2}(Br)}$ using CH_3OH as the solvent was recently reported,[89] and a Mn^{III} complex of the $\mathbf{H_2L^{OCO}}$ ligand (Scheme 1) was previously studied by Bellemin-Laponnaz and co-workers.[73] The complex was characterized by ESI-MS and EA. Dark brown crystals suitable for X-ray crystallography were obtained by slow evaporation of a concentrated CH_2Cl_2 solution. The solid-state structure of $\mathbf{MnL^{C2O2}(Br)}$ was recently reported,[89] however, certain metrical parameters differ due to the crystallization solvent. Thus, we will briefly describe the metrical parameters (Fig. S1 and Table S1†) in order to compare with the other solid-state structures herein. The Mn ion lies in a distorted square pyramidal geometry with the Mn center coordinated by two phenolate oxygen atoms (O1/O2) and two carbons of the NHC units (C7/C17) in equatorial positions. The anionic bromide ligand occupies the apical position, with the Mn atom 0.417 Å above the C_2O_2 ligand plane. The angle between the NHC and phenolate rings are 25° and 28° in the structure, and in addition the ligand backbone adopts an umbrella shape with an angle between the two NHC units of 32°. This is in contrast to the neutral Ni^{II} complex of the same ligand reported by us, in which the angle between the two NHC units is only 3°, the angle between the NHC and phenolate rings are ~9° and the complex is essentially flat.[70] In addition, the Ni–C_{NHC} bonds are significantly shorter (1.843 Å) in comparison to the Mn–C_{NHC} bonds in $\mathbf{MnL^{C2O2}(Br)}$ (2.03 Å). The ligand structural changes demonstrate significant binding flexibility, thereby accommodating different metal cations and different geometries.

The azido complex $\mathbf{MnL^{C2O2}(N_3)}$ was synthesized from a concentrated CH_3CN solution of $\mathbf{MnL^{C2O2}(Br)}$ in the presence of 1.5 equiv. of NaN_3 (Scheme 2). Solvent removal, addition of CH_2Cl_2 and filtration removed the excess NaN_3 affording $\mathbf{MnL^{C2O2}(N_3)}$ as a brown solid. IR ($\nu(N_3)$ = 2040 cm^{-1}), ESI-MS, and EA analysis confirmed product formation. Red/brown crystals suitable for X-ray diffraction were obtained *via* slow evaporation of a concentrated CH_3CN solution of $\mathbf{MnL^{C2O2}(N_3)}$. The solid-state structure of $\mathbf{MnL^{C2O2}(N_3)}$ is presented in Fig. 1 (see

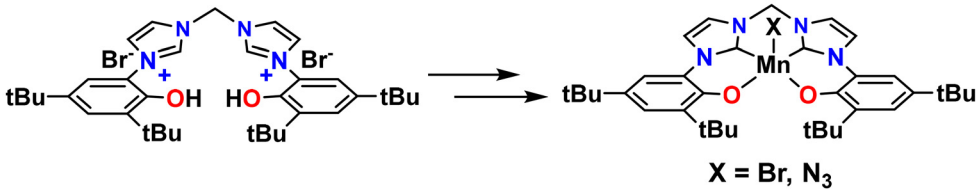

Scheme 2 Synthesis of Mn^{III} precursor complexes **MnL^{C2O2}(Br)** and **MnL^{C2O2}(N$_3$)**. Conditions: (X = Br) $Mn(OAc)_2$, NEt_3, 95% yield; (X = N_3) **MnL^{C2O2}(Br)**, NaN_3, 93% yield.

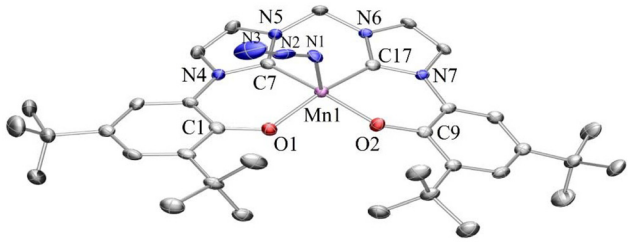

Fig. 1 POV-ray representation of **MnL^{C2O2}(N$_3$)**. Thermal ellipsoids shown at 50% probability level. Hydrogen atoms were omitted for clarity. Mn, pink; C, gray; O, red; N, blue. Select interatomic distances [Å]: Mn(1)–O(1): 1.889(2), Mn(1)–O(2): 1.885(2), Mn(1)–C(7): 2.026(2), Mn(1)–C(17): 2.022(2), Mn(1)–N(1): 2.110(4).

Table 1 UV-vis-NIR data for the indicated complexes[a]

Complex	λ_{max} [cm^{-1}] (ε [M^{-1} cm^{-1}])
MnL^{C2O2}(Br)	34 200 (11 660, sh), 29 200 (7550), 22 600 (2510, sh)
MnL^{C2O2}(N$_3$)	28 400 (3830, sh), 21 900 (1270, sh)
CrL^{C2O2}(N)	30 770 (6200), 28 000 (270)
[CrL^{C2O2}(N)]$^{+b}$	26 500 (7900, sh), 11 200 (2800)

[a] In CH_2Cl_2 solution. sh: shoulder. [b] 250 K.

ESI, Table S1† for selected crystallographic data). The distorted square pyramidal structure is similar to **MnL^{C2O2}(Br)**, with the azide ligand in the apical position, and an angle between the two NHC units of 33°. When dissolved in CH_2Cl_2 both **MnL^{C2O2}(Br)** and **MnL^{C2O2}(N$_3$)** display a brownish color and broad absorptions in their UV-vis-NIR spectra (Table 1 and Fig. S2†).

2.2. Attempted synthesis of Mn nitride complex MnL^{C2O2}(N)

With the two Mn^{III} complexes in hand, we next investigated two different synthetic methods to prepare the same Mn nitride product **MnL^{C2O2}(N)** (Scheme 1). Due to the susceptibility of nucleophilic attack at the methylene position between the two NHC rings of the ligand, we did not attempt to use NH_4OH/bleach as described by Carreira and co-workers.[90] Initially, we employed azide photolysis of **MnL^{C2O2}(N$_3$)** as this is a common method to produce nitrides (Scheme 3). Using the same protocol as one we had successfully used for Mn salen variants (λ = 312 nm, benzene solvent)[52] resulted in solution color changes, however, the Mn nitride complex **MnL^{C2O2}(N)** could not be isolated. Evans method analysis of the crude reaction mixture afforded a magnetic susceptibility of $\mu_{eff} \sim 4$ (or ~3 unpaired electrons) consistent with the presence

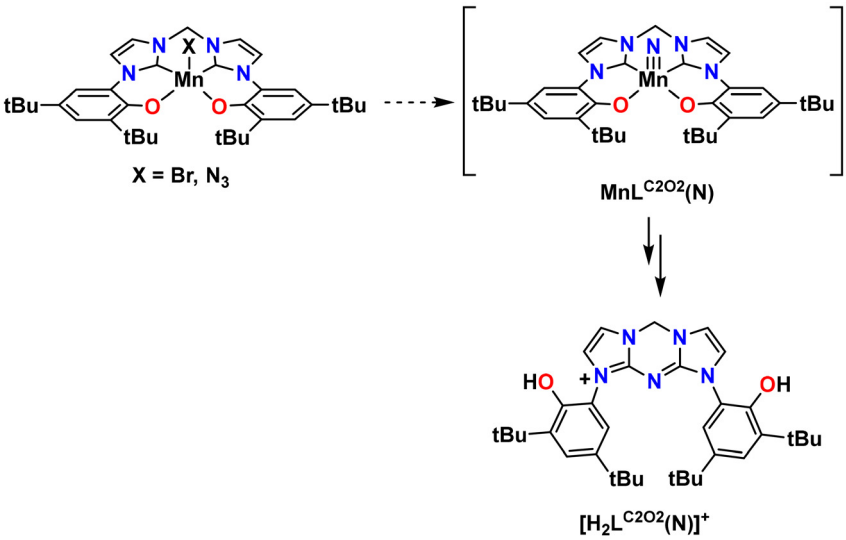

Scheme 3 Attempted synthesis of **MnL^{C2O2}(N)** from either **MnL^{C2O2}(N$_3$)** (λ = 312 nm, benzene solvent) or **MnL^{C2O2}(Br)** with a nitride exchange reagent **Mnsalen(N)** resulted in a mixture of products including the nitride inserted ligand **[H$_2$L^{C2O2}(N)]$^+$** (ESI-MS = 570.38 *m/z*).

of a paramagnetic Mn species, and an absence of the expected diamagnetic d^2 Mn^V nitride complex. While ESI-MS analysis of the crude reaction mixture showed the expected **MnL^{C2O2}(N)** peak at 624.3 *m*/*z*, attempted purification *via* chromatography and/or recrystallization was unsuccessful (*vide infra*). Irradiation at lower energy (λ > 350 nm), or low temperature (λ = 312 nm, CH_3CN, 235 K), resulted in no reaction.

We thus turned to a nitride exchange reaction, using a Mn^V salen nitride (**Mnsalen(N)**) complex as the nitride exchange reagent, which has been used to synthesize a variety of metal nitrides,[91–93] including nitride exchange to other Mn^{III} complexes (Scheme 3).[94] Mixing of 1 equiv. of the nitride exchange reagent with **MnL^{C2O2}(Br)** in CH_3CN resulted in the formation of a brown precipitate identified as **Mn^{III}salen(Br)** (ESI-MS, 321.04 *m*/*z*) which was removed *via* filtration. ESI-MS analysis of the filtrate exhibited the expected **MnL^{C2O2}(N)** peak at 624.3 *m*/*z* (Fig. S3†), however, we were again unable to isolate the desired nitride complex *via* chromatography and/or recrystallization. Attempting the nitride insertion reaction at low temperature (198 K, CH_2Cl_2) afforded the same result. Intriguingly, in these reactions a peak in the ESI-MS at 570.38 *m*/*z* indicated N-insertion into the ligand framework (Fig. S3†), pointing to a possible decomposition pathway for the initially formed **MnL^{C2O2}(N)** complex. Nitrido ligands have been reported to undergo intramolecular N-insertion into the ligand backbone of Fe,[16,20] Co,[38,95] U,[96] and Ni[41] complexes. In the majority of cases, population of antibonding π^* M≡N orbitals destabilizes the nitride, and thus intramolecular nitride insertion was unexpected for the putative d^2 Mn^V complex in this work. Meyer in a series of elegant studies has demonstrated intramolecular nitride insertion at a carbenic center in a series of Co[38] and Fe[16,20] complexes employing tripodal carbene-based ligands. Interestingly, the analogous Mn^V nitride complexes did not undergo the same insertion chemistry.[78]

2.3 Isolation of nitride insertion product

To further investigate the potential nitride insertion product, we solubilized the crude reaction mixture from a representative nitride exchange reaction in diethyl ether and washed with aqueous 10% HCl and then EDTA. Analysis by ESI-MS showed the loss of the Mn complex peak at 624.3 *m*/*z* (Fig. S4†). Further washing of a CH_3CN solution with hexane, and recrystallization by slow evaporation of CH_3CN/CH_2Cl_2 solution afforded pure ligand insertion product in 47% isolated yield. The same product can be isolated from the azide photolysis reaction, however in lower (~15%) yield. ^{1}H NMR of the product (Fig. S5†) showed the compound to be symmetric in solution (Fig. 2A), with the expected mass of 570.38 *m*/*z* (Fig. S6†). Further NMR analysis (^{13}C, ^{13}C DEPT and ^{1}H–^{13}C gHSQC NMR) provides confirmation of the structure in solution (Fig. S7–S9†). Interestingly, ^{1}H NMR in $CDCl_3$ results in broadened resonances indicative of hindered rotation of the phenol due to dynamics in the fast-exchange regime (Fig. S10†). Analysis of the product by X-ray crystallography showed that the nitride insertion product is a cation **[H$_2$L^{C2O2}(N)]$^+$** with chloride as the counterion (Fig. 2B). In addition, nitride insertion into both carbenic carbons has occurred, resulting in three fused rings including two imidazoles and a central triazone core. The nitride nitrogen (N1) exhibits similar short bond lengths to both carbenic carbons (N1–C7 and N1–C17: 1.335 and 1.334 Å respectively) and the three fused rings are essentially flat, with an 11° angle between the planes of the two imidazole rings. These structural features indicate the presence of a conjugated π system located across the N2–C7–N1–C17–N5 atoms (Fig. 2C). The hydrogen bond network involving the two phenols, a lattice water, and the chloride counterion ensures the secondary structure of the crystal (Fig. S11†). Interestingly, Bullock and co-workers have reported that H-atom abstraction from a bound NH_3 in $[Mn(dmpe)_2(CO)(NH_3)]^+$ (dmpe = 1,2-bis(dimethylphosphino)ethane) results in double insertion of the N-atom into the diphosphine ligand to form a cyclophosphazenium cation,[97] with theoretical calculations supporting insertion of an NH_x species rather than the nitride herein.

^{15}N isotopic labeling was employed to further investigate the N-atom insertion into the carbene ligand backbone. We used the ^{15}N-labeled nitride exchange reagent **Mnsalen(^{15}N)** in a reaction with **MnL^{C2O2}(Br)** and subsequent ESI-MS analysis showed a one Dalton *m*/*z* shift for the two ions at 571.4 (100%) and 625.3 (20%) (Fig. S12†) in comparison to the unlabeled reaction (Fig. S3†). The ^{15}N-inserted product **[H$_2$L^{C2O2}(^{15}N)]Cl** was isolated in a similar manner to the unlabeled analogue in a comparative yield (56%). To further confirm that the N-insertion is a result of intramolecular N-insertion from a transient **MnL^{C2O2}(N)** nitride complex, and not for example from an intermolecular process, we synthesized the ^{15}N-labeled azide complex **MnL^{C2O2}($^{14/15}$N$_3$)** using 50% terminally ^{15}N-labeled NaN_3. Photolysis of **MnL^{C2O2}($^{14/15}$N$_3$)** (λ = 312 nm) afforded a 1 : 1 mixture of N-inserted ligand products **[H$_2$L^{C2O2}(^{15}N)]Cl** and **[H$_2$L^{C2O2}(^{14}N)]Cl** by ESI-MS as well as an additional peak at 573.4 *m*/*z* likely corresponding to an O-inserted ligand product (Fig. S13†). The O-inserted product was not investigated further in this work. Overall, the two different isotopic labeling experiments provide further evidence that intramolecular N-atom insertion from an unstable **MnL^{C2O2}(N)** nitride complex results in formation of the **[H$_2$L^{C2O2}(N)]Cl** product.

2.4. Synthesis of the Cr nitride complex

Based on our previous work exploring the electronic structure and reactivity of the analogous Mn and Cr nitride complexes with salen ancillary ligands,[33,51,52] and the increased stability of the Cr derivatives more generally,[33,52] we investigated the preparation of the Cr nitride complex **CrL^{C2O2}(N)**. Following our previous work with salen ligands,[33] and the general preparation outlined by Bendix,[92] we added a solution of the **H$_2$L^{C2O2}·2HBr** ligand to an easily complexed $[Cr{\equiv}N]^{2+}$ synthon with labile auxillary ligands (CH_3CN and Cl^-) (Scheme 4).

A bright orange powder was isolated and confirmed to be the **CrL^{C2O2}(N)** complex based on IR (ν(N≡Cr) = 1025 cm^{-1}), ESI-MS (621.32 *m*/*z*, $[CrL + H]^+$, 100%; Fig. S14†), and X-ray crystallography. The UV-vis absorption spectrum of **CrL^{C2O2}(N)** displayed typical features of a d^1 Cr^V species in a square pyramidal

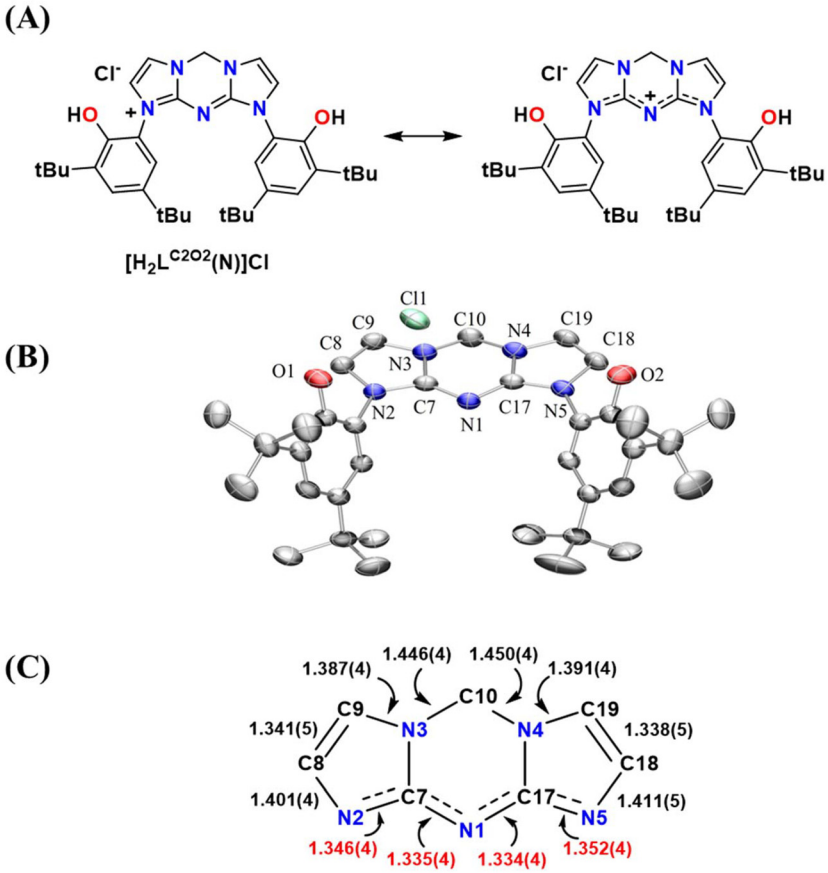

Fig. 2 (A) Structure of the nitride insertion product and charge delocalization. (B) POV-ray representation of $[H_2L^{C2O2}(N)]Cl$. Thermal ellipsoids shown at 50% probability level. Hydrogen atoms were omitted for clarity. (C) Selected bond lengths demonstrating the symmetric nature (and delocalization) of the product.

Scheme 4 Synthesis of the Cr nitride complex $CrL^{C2O2}(N)$ using the *in situ* generated $[Cr{\equiv}N]^{2+}$ synthon. See experimental section for details.

geometry, including an intense LMCT transition at 30 770 cm^{-1}, and a weak transition (ε < 300 M^{-1} cm^{-1}) at 20 800 cm^{-1} corresponding to a transition from the non-bonding $d^1{}_{xy}$ into empty d_{xz} or d_{yz} π^* orbitals (Fig. S15†). In addition, frozen solution X-band EPR measurements displayed an axial pattern, with simulation parameters ($g_\perp$ = 1.990, A^{53Cr} = 49; $g_{||}$ = 1.949, A^{53Cr} = 125) indicative of a d^1 Cr^V complex (Fig. 3).[98]

Single crystals suitable for X-ray diffraction were obtained by slow evaporation of a concentrated CH_2Cl_2/CH_3CN solution of $\mathbf{CrL^{C2O2}(N)}$ (Fig. 4 and Table S2†). The Cr ion is in a distorted square pyramidal environment with the Cr center coordinated to two phenolate oxygens (O1/O2), two NHC carbons (C7/C17), and the nitride ligand (N1). The Cr–nitride bond length of 1.558 Å is similar to that reported for other Cr^V nitrides.[33,99] The Cr center is shifted out of the ligand C_2O_2 plane by *ca.* 0.56 Å, which is slightly more than that reported for the salen analogues.[33,99] Similarly to the X-ray structures for both $\mathbf{MnL^{C2O2}(Br)}$ and $\mathbf{MnL^{C2O2}(N_3)}$ the ligand backbone for $\mathbf{CrL^{C2O2}(N)}$ adopts an umbrella shape with an angle between the two NHC units of 25°. Based on the marked difference in stability of the $\mathbf{MnL^{C2O2}(N)}$ and $\mathbf{CrL^{C2O2}(N)}$ complexes investigated herein we turned to theoretical calculations to further investigate their predicted electronic structure and reactivity differences.

2.5. Theoretical calculations on $CrL^{C2O2}(N)$ and $MnL^{C2O2}(N)$

The predicted metrical parameters for $\mathbf{CrL^{C2O2}(N)}$ were determined to be within ±0.03 Å of the experimental X-ray data

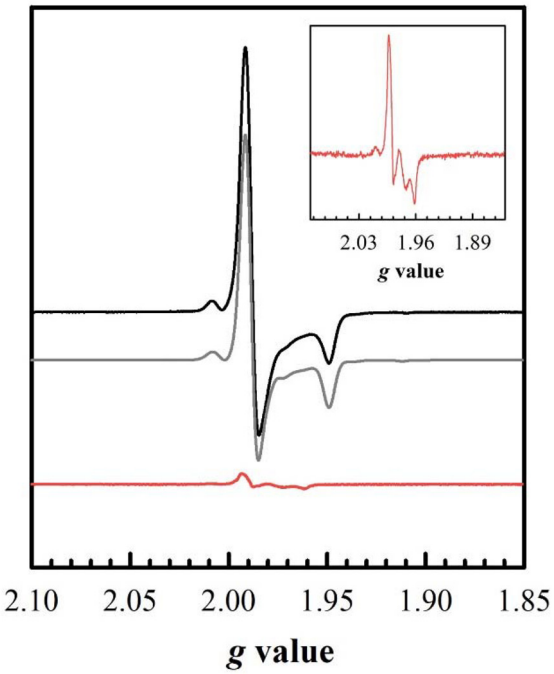

Fig. 3 Frozen solution EPR spectra of concentration-matched $\mathbf{CrL^{C2O2}(N)}$ (black) and oxidized $\mathbf{[CrL^{C2O2}(N)]^+}$ (red). Grey line indicates simulation of the experimental data for the neutral complex. Inset is a magnification of the oxidized complex signal. Conditions: 0.5 mM complex in CH_2Cl_2; 0.1 M TBAP; freq. = 9.64 GHz; power = 2.0 mW; T = 11 K.

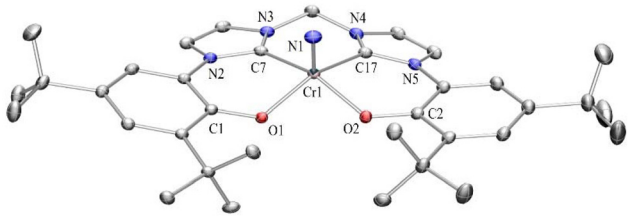

Fig. 4 POV-ray representation of $\mathbf{CrL^{C2O2}(N)}$. Thermal ellipsoids shown at the 50% probability level. Hydrogen atoms were omitted for clarity. Cr, pink; C, gray; O, red; N, blue. Select interatomic distances [Å]: Cr(1)–O(1): 1.935(1), Cr(1)–O(2): 1.919(1), Cr(1)–C(7): 2.058(1), Cr(1)–C(17): 2.062(1), Cr(1)–N(1): 1.558(1).

(Table 2). Similarly to the X-ray structure, a square pyramidal shape is predicted with the Cr atom out of plane towards the nitride (Fig. S16†). The Cr≡N bond length is predicted to be *ca.* 0.02 Å shorter in comparison to the X-ray data. Overall, the predicted structure for $\mathbf{MnL^{C2O2}(N)}$ (Fig. S17†) is similar to the Cr analogue, however, certain key differences are noted. For example, the computed Mn≡N bond length is *ca.* 0.03 Å shorter in comparison to Cr≡N, however the Mayer bond order for the Mn derivative is slightly lower (2.72 *vs.* 2.79). In addition, the Mn center is closer to the C_2O_2 plane, by *ca.* 0.05 Å (Table 2). By moving closer to the C_2O_2 plane the Mn center interacts more strongly with the carbene ligands, and

Table 2 X-ray metrical parameters (and predicted values in brackets) for $\mathbf{ML^{C2O2}(N)}$ in Å[a]

Complex	$\mathbf{CrL^{C2O2}(N)}$	$\mathbf{MnL^{C2O2}(N)}$
M–O1	1.937 (*1.921*)	(*1.924*)
M–O2	1.919 (*1.918*)	(*1.925*)
M–C7	2.058 (*2.063*)	(*1.979*)
M–C17	2.065 (*2.048*)	(*1.974*)
M–N1	1.558 (*1.536*)	(*1.505*)
M out of plane[b]	0.556 (*0.543*)	(*0.510*)

[a] Opt: B3LYP-D3, 6-31g*, PCM(CH_2Cl_2). [b] Distance from M to O1–O2–C7–C17 plane.

the predicted M–C(7/17) carbene bond lengths are *ca.* 0.08 Å shorter for the Mn complex in comparison to Cr. The shorter metal–carbene bond lengths in $\mathbf{MnL^{C2O2}(N)}$ likely facilitates the observed nitride insertion reactivity.

We compared the relative stability of $\mathbf{MnL^{C2O2}(N)}$ and $\mathbf{CrL^{C2O2}(N)}$ by investigating the initial insertion of the nitride into one of the M–C_{NHC} bonds. We considered this as the first step in the reaction pathway to eventually form the doubly inserted product $\mathbf{[H_2L^{C2O2}(N)]^+}$ (Scheme 3). The reaction pathway is shown in Fig. 5 with the triplet transition state (^{3}TS) calculated to be 24.17 kcal mol^{-1} higher in energy than the singlet $\mathbf{MnL^{C2O2}(N)}$ starting material. Note that by analyzing the potential energy surface (PES) for the reaction (Fig. S18†), it is apparent that the triplet energy surface (unpaired electrons in d^1_{xy} and $d^1_{xz/yz}$ rather than d^2_{xy}) is slightly lower in energy at the TS, with the ^{1}TS slightly higher in energy at 26.12 kcal mol^{-1}. Further analysis of the relative energies of the ^{1}TS *versus* the ^{3}TS using different DFT functionals/basis sets also predicts the ^{3}TS to be of lower energy (Table S3†), however such comparisons should be viewed with caution.[100] The nitride N is bridging the Mn–C_{NHC} bond at the TS (Fig. 5) supporting a *N*-migratory insertion pathway. The quintet nitride inserted Mn^{III} imido reaction product $\mathbf{MnL^{CNO2}}$ is stabilized by 9.72 kcal mol^{-1} relative to the $\mathbf{MnL^{C2O2}(N)}$ starting material (Fig. 5). In contrast, for the doublet $\mathbf{CrL^{C2O2}(N)}$ complex the ^{2}TS is calculated to be significantly higher at 35.22 kcal mol^{-1}, with the resulting quartet nitride inserted Cr^{III} imido reaction product $\mathbf{CrL^{CNO2}}$ de-stabilized by 3.03 kcal mol^{-1} relative to the $\mathbf{CrL^{C2O2}(N)}$ starting material (Fig. 5). Spin crossover to the quartet manifold is calculated to occur after the ^{2}TS (Fig. S18†). These calculations highlight the greater susceptibility of $\mathbf{MnL^{C2O2}(N)}$ to nitride insertion relative to $\mathbf{CrL^{C2O2}(N)}$, as observed experimentally. We note that Meyer *et al.* isolated a protonated imine reaction product in their studies,[16,38,101] however, we did not further evaluate this possibility as we have no experimental verification for either the imido or imine species herein. Further, we did not investigate the second N-carbene insertion to form the $\mathbf{[H_2L^{C2O2}(N)]^+}$ product due to the uncertainty in the identity of the final Mn product(s).

We next investigated the orbitals involved in the nitride insertion reaction to gain further insight. We analyzed the stabilization energy ($E^{(2)}$) in the equilibrium structures of

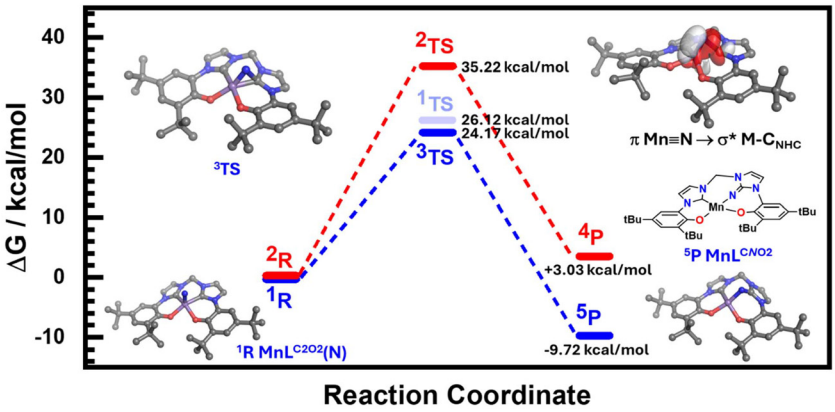

Fig. 5 Predicted reaction profile for nitride insertion from **ML^{C2O2}(N)** into the M–C_{NHC} bond to form the inserted product **ML^{CNO2}** (M = Mn (blue), Cr (red)). In the ^{3}TS for **MnL^{C2O2}(N)** (top left) the nitride N is bridging the Mn–C_{NHC} bond. Note the ^{1}TS is slightly higher in energy and spin crossover is predicted to occur before the TS (see Fig. S18 and Table S3†). The π M≡N → σ* M–C_{NHC} orbital interaction approaching the ^{3}TS is shown (top right). Predicted mono-inserted product **MnL^{CNO2}** bottom right. See Experimental section for calculation details.

ML^{C2O2}(N) (M = Mn, Cr) between different donating (filled) and accepting (empty) orbitals associated with the M≡N and M–C_{NHC} bonds using second-order perturbation theory (SOPT) from natural bond order (NBO) calculations.[102,103] This analysis predicts that while a donor–acceptor interaction occurs from filled NHC orbitals to the π* M≡N orbitals, the most significant interaction is in the opposite direction, and in particular π M≡N → σ* M–C_{NHC} (Table 3 and Fig. 5). It is interesting to note that the predicted donor–acceptor interactions are significantly increased for the Mn derivative in comparison to Cr (Table 3), which is in line with the shorter predicted M–C_{NHC} bond distance for the Mn derivative, and the observed reactivity. Further, we investigated the *change* in predicted orbital occupancy *via* NBO analysis for **MnL^{C2O2}(N)** as the N–Mn–C_{NHC} bond angle is decreased from the equilibrium structure (*ca.* 90°) to the TS (*ca.* 60°) along the reaction coordinate, and in line with the SOPT analysis, the most significant decrease occurs for the π M≡N orbitals, with a concomitant increase in occupancy for both σ* Mn–C_{NHC} and π* NHC (Fig. S19†). Overall, these calculations support the observed nitride insertion reactivity for the **MnL^{C2O2}(N)** complex, and lack thereof for **CrL^{C2O2}(N)**, and that the reactivity is primarily driven by nitride donation into σ*/π* orbitals associated with the NHC ligand.

Table 3 Second-order perturbation theory (SOPT) analysis of orbital interactions relevant to nitride insertion for **ML^{C2O2}(N)** (M = Mn, Cr)[a]

Reactivity	Donor → acceptor interaction	$E^{(2)}$ (kcal mol^{-1})	
		MnL^{C2O2}(N)	**CrL^{C2O2}(N)**
Nitride → NHC	π M≡N^b → σ* M–C_{NHC}	21.4	9.6
	π M≡N^b → π* NHC	6.0	—
NHC → Nitride	σ M–C_{NHC} → π* M≡N	9.3	3.7

[a] From NBO calculations (BP86-GD3/TZVP/PCM(CH_2Cl_2)) [b] Total of two π M≡N orbitals.

2.6. Oxidation of Cr nitride complex

Upon isolation and characterization of the neutral nitride complex **CrL^{C2O2}(N)** we next investigated its oxidation chemistry to better understand the stability and electronic structure of the one-electron oxidized form. Cyclic voltammetry experiments exhibited a *quasi*-reversible one-electron redox process at 0.14 V *vs.* Fc^+/Fc (Fig. 6), with no other redox processes observed in the electrochemical window (Fig. S20†). Based on previous work, additional redox processes would be expected

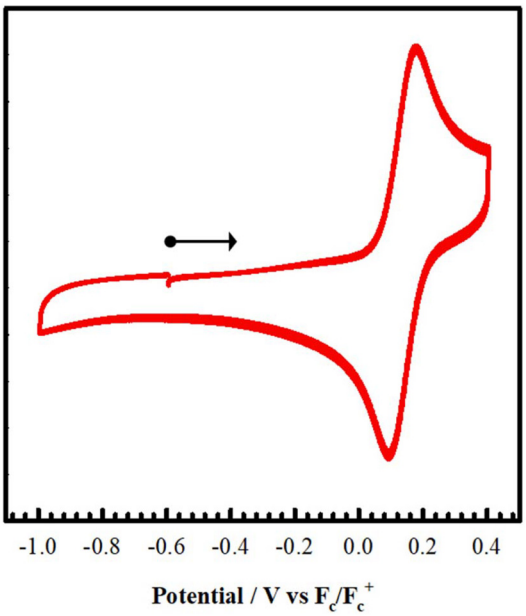

Fig. 6 Cyclic voltammogram of **CrL^{C2O2}(N)** showing a *quasi*-reversible redox process at 0.14 V *vs.* Fc^+/Fc. Peak to peak difference ($E_{pa} - E_{pc}$ = 0.093 V). $E_{pa} - E_{pc}$ = 0.070 V for Fc^+/Fc. Conditions: 0.5 mM complex, CH_2Cl_2, 0.1 M tetrabutylammonium perchlorate (TBAP), scan rate = 100 mV s^{-1}, 298 K.

in the case of ligand-based oxidation.[33,70] Interestingly, this redox potential is between that reported for **CrNSal**^{OiPr} ($E_{1/2}$ = 0.38 V *vs.* Fc^+/Fc) and **CrNSal**^{NMe2} ($E_{1/2}$ = −0.04 V *vs.* Fc^+/Fc) with the former characterized as a Cr^{VI} species and the latter as a Cr^{V} ligand radical, upon oxidation.[33]

Based on the *quasi*-reversible oxidation process, and the relatively low redox potential, we further investigated the bulk oxidation of **CrL**^{C2O2}**(N)** to **[CrL**^{C2O2}**(N)]**$^+$ with tris(2,4-dibromophenyl)aminium hexafluoroantiminoate ([N$(C_6H_3Br_2)_3]^{\bullet+}[SbF_6]^-$; $E_{1/2}$ = 1.1 V *vs.* Fc^+/Fc).[104] Upon sequential addition of a solution of the oxidant to **CrL**^{C2O2}**(N)** at 253 K in CH_2Cl_2 a new band is observed at 26 500 cm^{-1} along with a lower energy transition at 11 200 cm^{-1} (2800 M^{-1} cm^{-1}) (Fig. 7). The oxidized complex is stable for at least one hr at 253 K (Fig. S21†). The UV-vis-NIR spectrum of **[CrL**^{C2O2}**(N)]**$^+$ is similar to that reported for the Cr^{VI} nitride complexes with salen ancillary ligands, in which a comparable low energy feature was assigned as a ligand-to-metal charge transfer (LMCT) band.[33] It is unlikely that the 11 200 cm^{-1} transition is a ligand radical intervalence charge transfer (IVCT) band as the single one-electron redox feature discounts a Class II regime, and analysis of the band properties ($\Delta\nu_{1/2}$ = 6500 cm^{-1}, ε = 2800 M^{-1} cm^{-1}) are not in line with a Class III ligand radical ($\Delta\nu_{1/2} \leq 2000$ cm^{-1}, $\varepsilon > 5000$ M^{-1} cm^{-1}).[105]

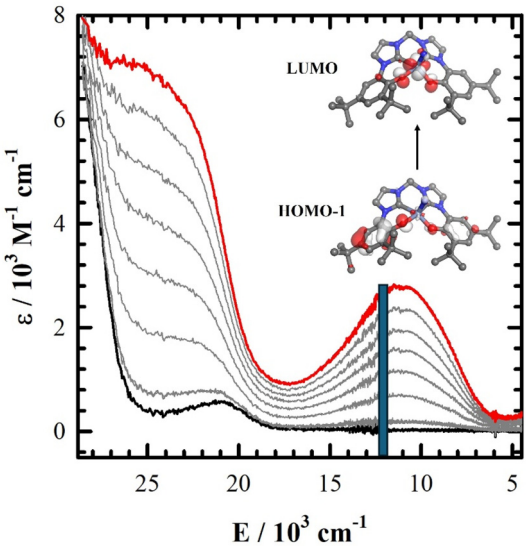

Fig. 7 Chemical oxidation of **CrL**^{C2O2}**(N)** using $[N(C_6H_3Br_2)_3]^{\bullet+}[SbF_6]^-$ monitored by UV-vis-NIR spectroscopy. Black: neutral; red: oxidized. Intermediate grey lines represent increasing aliquots of oxidant added until one equiv. was reached. Conditions: 0.45 mM complex, CH_2Cl_2, 253 K. Blue bar represents most intense TD-DFT predicted low energy transition at 12 098 cm^{-1}, and donor/acceptor orbitals indicating LMCT character for the Cr^{VI} electronic structure. See Experimental section for calculation details.

EPR analysis of **[CrL**^{C2O2}**(N)]**$^+$ shows *ca.* 5% signal intensity in comparison to a concentration-matched sample of **CrL**^{C2O2}**(N)**, with the remaining signal mostly due to unoxidized **CrL**^{C2O2}**(N)** (Fig. 3). Loss of the EPR signal can be attributed to (1) formation of a d^0 Cr^{VI} complex, (2) an antiferromagnetically coupled Cr^{V} ligand radical species (S = 0, open-shell singlet), or (3) a ferromagnetically coupled Cr^{V} ligand radical species (S = 1, triplet) exhibiting large zero-field splitting.[106,107] We further investigated the predicted change in metrical parameters upon oxidation and relative energy of the different plausible electronic structures using theoretical calculations. The metal oxidized Cr^{VI} species was predicted to be lowest in energy, with the antiferromagnetically coupled Cr^{V} ligand radical species (broken-symmetry, BS) higher in energy by +6.03 kcal mol^{-1}, and the ferromagnetically coupled Cr^{V} ligand radical species (triplet, T) highest in energy by +13.95 kcal mol^{-1} (Table 4). The ligand radical is predicted to

Table 4 Predicted relative energies for possible electronic structures of **[CrL**^{C2O2}**(N)]**$^+$ and associated time-dependent density functional theory (TD-DFT) predicted low energy transitions[a]

Electronic structure	Relative energy (kcal mol^{-1})	Predicted low energy transition
[CrL^{C2O2}**(N)]**$^+$ (S)	0.00	HOMO/HOMO−1 → LUMO (12 098 cm^{-1}, f = 0.0870)
[CrL^{C2O2}**(N)]**$^+$ (BS)	+6.03	HOMO/HOMO−1 → LUMO (4727 cm^{-1}, f = 0.0521)
[CrL^{C2O2}**(N)]**$^+$ (T)	+13.95	HOMO/HOMO−1 → LUMO (3957 cm^{-1}, f = 0.0949)

[a] Single point: BP86-GD3/TZVP/PCM(CH_2Cl_2).

Table 5 Predicted metrical parameters for **CrL**^{C2O2}**(N)** and **[CrL**^{C2O2}**(N)]**$^+$ in Å[a]

Complex	**CrL**^{C2O2}**(N)**	**[CrL**^{C2O2}**(N)]**$^+$ (S)	**[CrL**^{C2O2}**(N)]**$^+$ (T)	**[CrL**^{C2O2}**(N)]**$^+$ (BS)
Cr–O1	(*1.921*)	(*1.819*)	(*1.988*)	(*1.960*)
Cr–O2	(*1.918*)	(*1.802*)	(*1.886*)	(*1.876*)
Cr–C7	(*2.063*)	(*2.044*)	(*2.059*)	(*2.062*)
Cr–C17	(*2.048*)	(2.072)	(2.024)	(*2.028*)
Cr–N1	(*1.536*)	(*1.516*)	(*1.531*)	(*1.532*)
Cr out of plane[b]	(*0.543*)	(*0.472*)	(*0.505*)	(*0.491*)

[a] Opt: B3LYP-D3, 6-31g*, PCM(CH_2Cl_2). [b] Distance from Cr to O1–O2–C7–C17 plane.

be localized to form a phenoxyl/phenolate species for the BS and T solutions (Fig. S22†), with the expected difference in Cr–O1/Cr–O2 bond lengths (Table 5). We further investigated the predicted low energy transitions for the three possible electronic structures based on the experimentally observed UV-vis-NIR feature at 11 200 cm^{-1} (Fig. 7). Both ligand radical electronic structures (BS, T) predict low energy transitions in the NIR (Table 4), and no transitions of appreciable intensity are observed experimentally in this energy region (Fig. 7). However, the Cr^{VI} singlet solution correctly predicts a ligand to metal charge transfer (LMCT) transition at 12 098 cm^{-1} (Fig. 7 and Table 4), providing further support that this is the correct electronic structure of $[\mathbf{CrL^{C2O2}(N)}]^+$.

3. Summary

In this work we studied the synthesis and properties of the Mn and Cr nitrides of a tetradentate bis-phenol bis-N-heterocyclic carbene ligand $\mathbf{H_2L^{C2O2}}$. The tetradentate platform of $\mathbf{H_2L^{C2O2}}$ exhibits similarities to the common salen analogue $\mathbf{H_2Sal^R}$ (Scheme 1), however the different donating/accepting properties of the NHC units in comparison to imine functionalities of the salen framework provide for an interesting comparison. Indeed, while the Mn^V nitride salen complexes have been reported extensively,[108,109] the Mn^V nitride $\mathbf{MnL^{C2O2}(N)}$ could not be isolated herein. Our results suggest that $\mathbf{MnL^{C2O2}(N)}$ forms, yet is unstable, and the nitride rapidly inserts into a Mn–C_{NHC} bond. A second insertion reaction results in the isolation of the doubly inserted ligand product $[\mathbf{H_2L^{C2O2}(N)}]^+$. Interestingly, the Cr analogue $\mathbf{CrL^{C2O2}(N)}$ can be readily prepared and does not exhibit nitride N-insertion reactivity. Theoretical investigations predict that the transition state for the first N-insertion is *ca.* 10 kcal mol^{-1} lower in energy for the Mn derivative, and the reactivity is primarily driven by nucleophilic attack of the terminal nitride on the carbene (π M≡N → σ^* M–C_{NHC}). Theoretical calculations predict the Mn–C_{NHC} bond lengths to be ~0.08 Å shorter in comparison to the Cr–C_{NHC} bonds for $\mathbf{ML^{C2O2}(N)}$ (M = Mn, Cr) (Table 2), providing rationale for the facile N-insertion reactivity observed for $\mathbf{MnL^{C2O2}(N)}$. In addition, the observed N-insertion reactivity is in accord with the general lower stability and more extensive reactivity of Mn nitrides in comparison to Cr nitrides.[33,52,91–93] Finally, we investigated the one-electron oxidation of the $\mathbf{CrL^{C2O2}(N)}$ complex, and determined that metal-based oxidation occurs to form the d^0 Cr^{VI} product $[\mathbf{Cr^{VI}L^{C2O2}(N)}]^+$.

4. Experimental section

4.1. Materials and methods

All chemicals were of the highest quality grade and purified whenever necessary. The ligand $\mathbf{H_4L^{C2O2}Br_2}$ was synthesized following a literature procedure.[70] The atom-transfer reagents Mnsalen(N) and $CrCl_3(THF)_3$ were also prepared according to published protocols.[90,92] Dichloromethane and acetonitrile were dried by refluxing over calcium hydride and distilled prior to use. The tris(2,4-dibromophenyl)aminium hexafluoroantimonate radical oxidant $[N(C_5H_3Br_2)_3][SbF_6]$ was synthesized according to published protocols.[110] Electronic spectra were obtained using a Cary 5000 spectrophotometer. Mass spectrometry (ESI positive mode) was performed on an Agilent 6210 TOF ESI-MS system. ^1H nuclear magnetic resonance (NMR) spectroscopy as well as magnetic susceptibility *via* Evans Method were carried out on a Bruker AVANCE III 500 MHz instrument. Elemental analysis (C, H, N) were performed at Simon Fraser University on a Carlo Erba EA1110 CHN elemental analyser. All electron paramagnetic resonance (EPR) were recorded on a Bruker EMXplus spectrometer operating with a premium X-band microwave bridge and an HS resonator. EPR spectra were simulated using the EasySpin package in Matlab.[111] Solid state infrared spectra (IR) were measured on a Thermo Nicolet Nexus 670 FT-IR spectrometer equipped with a Pike MIRacle attenuated total reflection (ATR) sampling accessory. Cyclic voltammetry (CV) was performed on a PAR-263A potentiometer equipped with a silver wire reference electrode, a platinum disk counter electrode and glassy carbon working electrode. Tetrabutylammonium perchlorate (0.1 M) was used as the supporting electrolyte, and decamethylferrocene was used as an internal standard in CH_2Cl_2.[112] One-electron processes were confirmed *via* comparison of the electrochemical response of one equiv. of the Cr complex *versus* decamethylferrocene.

4.2. Synthesis

4.2.1 Synthesis of $\mathbf{MnL^{C2O2}(Br)}$. This procedure differs slightly from that recently reported.[89] The pro-ligand $\mathbf{H_4L^{C2O2}Br_2}$ (152 mg, 212 μmol) was suspended in a solution of manganese(II) acetate tetrahydrate (52.1 mg, 213 μmol) in dry acetonitrile (25 mL). Triethylamine (120 μL, 0.86 mmol) was added and the resulting mixture was stirred at 80 °C for 3 h. The solution gradually homogenized as it turned a brown color. It was then evaporated and the crude product was solubilized in toluene, then filtered over Celite. The filtrate was evaporated and dried under high vacuum overnight to afford $\mathbf{MnL^{C2O2}(Br)}$ as a brown solid (147 mg, 95%). MS (HRMS): m/z = 609.29 $[MnL - Br]^+$. Anal. calcd (%) $C_{35}H_{46}MnBrN_4O_2{\cdot}0.5H_2O$: C 60.17, H 6.78, N 8.02; found (%): C 60.19, H 7.25, N 7.68. Dark brown crystals suitable for X-Ray diffraction were obtained by slow evaporation of a concentrated dichloromethane solution of $\mathbf{MnL^{C2O2}(Br)}$.

4.2.2 Synthesis of $\mathbf{MnL^{C2O2}(N_3)}$. $\mathbf{MnL^{C2O2}(Br)}$ (135 mg, 196 μmol) was solubilized in a solution acetonitrile (8 mL) and H_2O (1.5 mL). A solution of sodium azide 1 M in H_2O (215 μL, 215 μmol) was added dropwise and the mixture was stirred at room temperature for 1 h. A large spatula of sodium sulfate was added and the volatiles were removed under vacuum. The crude product was solubilized in dichloromethane and filtered over Celite. The filtrate was evaporated to afford $\mathbf{MnL^{C2O2}(N_3)}$ as a brown solid (122 mg, 93%). IR: $\nu(N_3)$ = 2040 cm^{-1}. ESI-MS: m/z = 609.30 $[MnL - N_3]^+$. Anal. calcd (%) $C_{35}H_{46}MnBrN_7O_2$: C 64.50,

H 7.11, N 15.04; found (%): C 64.11, H 7.23, N 14.75. Red/brown crystals suitable for X-Ray diffraction were obtained by slow evaporation of a concentrated acetonitrile solution of **MnL^{C2O2}(N$_3$)**.

4.2.3 Synthesis of inserted ligand [H$_2$L^{C2O2}(N)]Cl. A solution of **MnL^{C2O2}(Br)** (102.8 mg, 149 μmol) in dichloromethane (8 mL) was added dropwise to **Mnsalen(N)** (50.4 mg, 150 μmol) suspended in dichloromethane (5 mL). A brown precipitate formed instantly and the solution was stirred under air for 2 h. The precipitate was removed by filtration and the brown filtrate was evaporated. The crude mixture was solubilized in 20 mL of diethyl ether. The organic phase was washed three times with a 10% HCl solution, then three times by a saturated H_2O solution of tetrasodium EDTA, followed by two times with H_2O and one final time with brine. The organic phase was dried over Na_2SO_4 and evaporated. The resulting pale brown solid was solubilized in acetonitrile and washed 5 times with hexanes. Finally, the acetonitrile solution was evaporated and dried under high vacuum overnight, affording **[H$_2$L^{C2O2}(N)]Cl** as a beige powder (42.3 mg, 47%). ^{1}H NMR (500 MHz, CD_3OD) δ 1.28 (s, 18H, *t*-Bu), 1.34 (s, 18H, *t*-Bu), 6.30 (s, 2H, CH_2), 7.11 (s, 2H, aryl–H), 7.29 (s, 2H, aryl–H), 7.32 (s, 2H, aryl–H), 7.41 (s, 2H, aryl–H). ^{13}C (375 MHz) δ 31.04 (CH_3), 32.64 (CH_3), 36.14 ($C_{quat.}$), 37.27 ($C_{quat.}$), 61.65 (CH_2), 115.70 (CH), 121.35 (CH), 123.37 (CH), 125.40 ($C_{quat.}$), 127.19 (CH), 141.91 ($C_{quat.}$), 145.18 ($C_{quat.}$), 148.26 ($C_{quat.}$), 149.96 ($C_{quat.}$). MS (HRMS): m/z = 570.38 [M − Cl]$^+$.

4.2.4 Synthesis of inserted ligand [H$_2$L^{C2O2}(^{15}N)]Cl. A solution of **MnL^{C2O2}(Br)** (101.7 mg, 147 μmol) in dichloromethane (7 mL) was added dropwise to **Mnsalen(^{15}N)** (50.0 mg, 149 μmol) suspended in dichloromethane (4 mL). A brown precipitate formed instantly and the solution was stirred under air for 3 h. The precipitate was removed by filtration and the filtrate was evaporated. The crude mixture was solubilized in diethyl ether. The organic phase was washed three times by a 10% HCl solution, then three times by a saturated H_2O solution of tetrasodium EDTA, followed by two times with H_2O and one final time with brine. The organic phase is dried over Na_2SO_4 and evaporated. The resulting pale brown solid was solubilized in acetonitrile and washed 5 times with hexanes. Finally, the acetonitrile solution was evaporated and dried under high vacuum overnight, affording **[H$_2$L^{C2O2}(^{15}N)]Cl** as a beige powder (50.0 mg, 56%). MS (HRMS): m/z = 571.38 [M − Cl]$^+$. Colorless crystals suitable for X-Ray diffraction were obtained by slow evaporation of a CH_2Cl_2/CH_3CN (1 : 1 v/v) solution of **[H$_2$L^{C2O2}(^{15}N)]Cl**.

4.2.5 Synthesis of CrL^{C2O2}(N). The procedure was adapted from a previous report by Bendix.[92] A solution of $CrCl_3(THF)_3$ (219.1 mg, 585 μmol) was prepared in dry acetonitrile (5 mL) under N_2 atmosphere in a glovebox. To this solution **Mnsalen (N)** was then added (193.4 mg, 577 μmol) while stirring. The purple solution immediately turned brown and a brown precipitate formed. The mixture was stirred under air at room temperature for 1 h then was filtered over Celite to afford a yellow-brown solution of [N≡Cr]$^{2+}$ complex. The solution containing the [N≡Cr]$^{2+}$ complex was then added dropwise to an ethanol solution (40 mL) of **H$_4$L^{C2O2}Br$_2$** (376.0 mg, 523 μmol) and Et_3N (300 μL, 2.15 mmol) stirred at 60 °C. The resulting mixture was stirred under reflux under air overnight then evaporated. The orange brown crude solid was suspended in cold methanol, collected and washed with cold methanol to afford **CrL^{C2O2}(N)** as a bright orange powder (127.6 mg, 39%). IR: ν(N≡Cr) = 1025 cm^{-1}. MS (HRMS): m/z = 621.32 [CrL + H]$^+$. Orange crystals suitable for X-Ray diffraction were obtained by slow evaporation of a concentrated solution of **CrL^{C2O2}(N)** in a dichloromethane/acetonitrile solvent system.

4.2.6 Synthesis of CrL^{C2O2}(^{15}N). Identical procedure to **2.5** except **Mnsalen(^{15}N)** used. Yield 57.5 mg, 35%. IR: ν(^{15}N≡Cr) = 998 cm^{-1}. MS (HRMS): m/z = 622.31 [CrL + H]$^+$.

4.3. X-ray crystallography

Diffraction data for brown needle single crystals of **MnL^{C2O2}Br**, red blade crystals of **MnL^{C2O2}(N$_3$)**, and orange prism crystals of **CrL^{C2O2}(N)** were collected at the University of British Columbia (Canada) by Dr Brian Patrick on a Bruker X8 Apex II diffractometer with graphite monochromated Mo-Kα radiation (λ = 0.71073 Å) at 296 K. Data were integrated using the Bruker SAINT software package (Bruker, V8.40B, 2016) and absorption corrections were performed using the multiscan technique SADABS-2016/2 (Bruker, 2016/2). The structures were solved by Dr Nicholas Hein and Jason Pulfer using the SHELX software[113] implemented by Olex2.[114] All non-hydrogen atoms were anisotropically refined and hydrogen atoms were placed at calculated positions and refined as riding atoms with isotropic displacement parameters. It is noted that for **MnL^{C2O2}(N$_3$)** a residual peak was modeled at 2.55 Å as a Br from the starting material. The refined occupancies are azide (0.967(3)) and Br (0.033(3)). Further data is shown in Tables S1 and S2. Diffraction data for the yellow prism single crystal of solvated **[H$_2$L^{C2O2}(N)]Cl** were collected at Université de Grenoble Alpes (France) by Dr Christian Philouze on a Bruker-AXS-Enraf-Nonius Kappa Apex II diffractometer with multilayer mirrors monochromated Mo-Kα radiation (λ = 0.71073 Å) from an Incoatec high brilliance micro-source at 210 K. Data were integrated using the Bruker EvalCCD software package and absorption corrections were performed using the multiscan technique SADABS-2004/1. The structure was solved by using the SHELX software[113] implemented by Olex2.[114] All non-hydrogen atoms were anisotropically refined and hydrogen atoms were placed at calculated positions and refined as riding atoms with isotropic displacement parameters. The structure displays a solvation site which may be modeled with two dichloromethane and one acetonitrile molecules spread over 3 different positions and with respective partial occupancy: 0.3968, 0.35167 and 0.25 Further data is shown in Table S1 and Fig. S11.† The crystallographic data for the new structures have been deposited with Cambridge Crystallographic Data Centre as supplementary publication no. CCDC 2359452, 2359453, 2359455, and 2359456.†

4.4. Theoretical calculations

Geometry optimizations were all performed using the Gaussian 16 program (Revision A.03)[115] employing the B3LYP

functional, the D3 dispersion correction[116] in combination with the 6-31g* basis set. Frequency calculations performed on the same functional/basis set confirmed optimized structures were at a global minimum. Single-point calculations as well as time-dependant DFT calculations were performed using the BP86-GD3 functional and the TZVP basis set of Ahlrichs.[117,118] Natural bond order (NBO) calculations were completed using the single-point calculations in the Gaussian 16 program.[119] For reaction profile calculations single-point energies were converted to Gibbs free energies using corrections from the frequency calculations on the optimized coordinates. Calculated transition states were confirmed to have one negative frequency associated with N–C bond formation. All calculations employed a polarizable continuum model (PCM) for CH_2Cl_2 (ε = 8.93) for all atoms.[120]

Data availability

Compound characterization, ^{1}H NMR and ESI-MS data, as well as X-ray crystallography details are available in the ESI.† Calculation data is compiled in a zip folder.

Conflicts of interest

There are no conflicts to declare.

Acknowledgements

This work was supported by Natural Sciences and Engineering Research Council (NSERC) Discovery Grants (RGPIN-2019-06749 and RGPAS-2019-00054 to T. S.). Digital Alliance Canada is thanked for access to computational resources. D. M. acknowledges Mitacs Canada for a Globalink Fellowship (FR43327). Dr Brian Patrick is thanked for assistance with solving the X-ray structures. This work is also supported by the French National Research Agency in the framework of the "Investissements d'avenir" program (ANR-15-IDEX-02) and Labex ARCANE and CBH-EUR-GS (ANR-17-EURE-0003) for financial support. The NanoBio-ICMG platforms (FR 2607) are acknowledged for their support.

References

1 D. V. Yandulov and R. R. Schrock, Catalytic reduction of dinitrogen to ammonia at a single molybdenum center, *Science*, 2003, **301**, 76.
2 S. J. K. Forrest, B. Schluschaß, E. Y. Yuzik-Klimova and S. Schneider, Nitrogen Fixation via Splitting into Nitrido Complexes, *Chem. Rev.*, 2021, **121**, 6522.
3 G. Ertl, *Catalytic Ammonia Synthesis*, Plenum, New York, 1991.
4 M. N. Cosio and D. C. Powers, Prospects and challenges for nitrogen-atom transfer catalysis, *Nat. Rev. Chem.*, 2023, **7**, 424.
5 J. J. Curley, E. L. Sceats and C. C. Cummins, A Cycle for Organic Nitrile Synthesis via Dinitrogen Cleavage, *J. Am. Chem. Soc.*, 2006, **128**, 14036.
6 J. Du Bois, C. S. Tomooka, J. Hong and E. M. Carreira, Nitridomanganese(v) Complexes: Design, Preparation, and Use as Nitrogen Atom-Transfer Reagents, *Acc. Chem. Res.*, 1997, **30**, 364.
7 P. F. Kuijpers, J. I. van der Vlugt, S. Schneider and B. de Bruin, Nitrene Radical Intermediates in Catalytic Synthesis, *Chem. – Eur. J.*, 2017, **23**, 13819.
8 K. M. Carsch, I. M. DiMucci, D. A. Iovan, A. Li, S.-L. Zheng, C. J. Titus, S. J. Lee, K. D. Irwin, D. Nordlund, K. M. Lancaster and T. A. Betley, Synthesis of a copper-supported triplet nitrene complex pertinent to copper-catalyzed amination, *Science*, 2019, **365**, 1138.
9 S. Kim, D. Kim, S. Y. Hong and S. Chang, Tuning Orbital Symmetry of Iridium Nitrenoid Enables Catalytic Diastereo- and Enantioselective Alkene Difunctionalizations, *J. Am. Chem. Soc.*, 2021, **143**, 3993.
10 Y. Gao, V. Carta, M. Pink and J. M. Smith, Catalytic Carbodiimide Guanylation by a Nucleophilic, High Spin Iron(ii) Imido Complex, *J. Am. Chem. Soc.*, 2021, **143**, 5324.
11 B. Bagh, D. L. J. Broere, V. Sinha, P. F. Kuijpers, N. P. van Leest, B. de Bruin, S. Demeshko, M. A. Siegler and J. I. van der Vlugt, Catalytic Synthesis of N-Heterocycles via Direct C(sp3)–H Amination Using an Air-Stable Iron(iii) Species with a Redox-Active Ligand, *J. Am. Chem. Soc.*, 2017, **139**, 5117.
12 T. Schmidt-Räntsch, H. Verplancke, J. N. Lienert, S. Demeschko, M. Otte, G. P. Van Trieste III, K. A. Reid, J. H. Reibenspies, D. C. Powers, M. C. Holthausen and S. Schneider, Nitrogen Atom Transfer Catalysis by Metallonitrene C–H Insertion: Photocatalytic Amidation of Aldehydes, *Angew. Chem., Int. Ed.*, 2022, **61**, e202115626.
13 M. Goswami, V. Lyaskovskyy, S. R. Domingos, W. J. Buma, S. Woutersen, O. Troeppner, I. Ivanovic-Burmazovic, H. J. Lu, X. Cui, X. P. Zhang, E. J. Reijerse, S. DeBeer, M. M. van Schooneveld, F. F. Pfaff, K. Ray and B. de Bruin, Characterization of Porphyrin-Co(iii)-'Nitrene Radical' Species Relevant in Catalytic Nitrene Transfer Reactions, *J. Am. Chem. Soc.*, 2015, **137**, 5468.
14 J. J. Scepaniak, C. S. Vogel, M. M. Khusniyarov, F. W. Heinemann, K. Meyer and J. M. Smith, Synthesis, Structure, and Reactivity of an Iron(v) Nitride, *Science*, 2011, **331**, 1049.
15 J. F. Berry, E. Bill, E. Bothe, S. D. George, B. Mienert, F. Neese and K. Wieghardt, An octahedral coordination complex of iron(vi), *Science*, 2006, **312**, 1937.
16 M. Keilwerth, L. Grunwald, W. Mao, F. W. Heinemann, J. Sutter, E. Bill and K. Meyer, Ligand Tailoring Toward an Air-Stable Iron(v) Nitrido Complex, *J. Am. Chem. Soc.*, 2021, **143**, 1458.

17 N. B. Thompson, M. T. Green and J. C. Peters, Nitrogen Fixation via a Terminal Fe(IV) Nitride, *J. Am. Chem. Soc.*, 2017, **139**, 15312.
18 A. K. Maity, J. Murillo, A. J. Metta-Magaña, B. Pinter and S. Fortier, A Terminal Iron(IV) Nitride Supported by a Super Bulky Guanidinate Ligand and Examination of Its Electronic Structure and Reactivity, *J. Am. Chem. Soc.*, 2017, **139**, 15691.
19 M. Keilwerth, W. Mao, M. Malischewski, S. A. V. Jannuzzi, K. Breitwieser, F. W. Heinemann, A. Scheurer, S. DeBeer, D. Munz, E. Bill and K. Meyer, The synthesis and characterization of an iron(VII) nitrido complex, *Nat. Chem.*, 2024, **16**, 514.
20 M. Keilwerth, W. Mao, S. A. V. Jannuzzi, L. Grunwald, F. W. Heinemann, A. Scheurer, J. Sutter, S. DeBeer, D. Munz and K. Meyer, From Divalent to Pentavalent Iron Imido Complexes and an Fe(V) Nitride via N–C Bond Cleavage, *J. Am. Chem. Soc.*, 2023, **145**, 873.
21 E. D. Badding, S. Srisantitham, D. A. Lukoyanov, B. M. Hoffman and D. L. M. Suess, Connecting the geometric and electronic structures of the nitrogenase iron-molybdenum cofactor through site-selective 57Fe labelling, *Nat. Chem.*, 2023, **15**, 658.
22 Y. Kim, A. Sridharan and D. L. M. Suess, The Elusive Mononitrosylated Fe4S4 Cluster in Three Redox States, *Angew. Chem., Int. Ed.*, 2022, **61**, e202213032.
23 L. Grunwald, M. Clémancey, D. Klose, L. Dubois, S. Gambarelli, G. Jeschke, M. Wörle, G. Blondin and V. Mougel, A complete biomimetic iron-sulfur cubane redox series, *Proc. Natl. Acad. Sci. U. S. A.*, 2022, **119**, e2122677119.
24 A. Sridharan, A. C. Brown and D. L. M. Suess, A Terminal Imido Complex of an Iron–Sulfur Cluster, *Angew. Chem., Int. Ed.*, 2021, **60**, 12802.
25 A. McSkimming and D. L. M. Suess, Dinitrogen binding and activation at a molybdenum–iron–sulfur cluster, *Nat. Chem.*, 2021, **13**, 666.
26 J. M. Smith, Reactive Transition Metal Nitride Complexes, *Prog. Inorg. Chem.*, 2014, **58**, 417.
27 R. A. Eikey and M. M. Abu-Omar, Nitrido and imido transition metal complexes of Groups 6–8, *Coord. Chem. Rev.*, 2003, **243**, 83.
28 J. F. Berry, Terminal Nitrido and Imido Complexes of the Late Transition Metals, *Comments Inorg. Chem.*, 2009, **30**, 28.
29 C. E. Laplaza and C. C. Cummins, Dinitrogen Cleavage by a 3-Coordinate Molybdenum(III) Complex, *Science*, 1995, **268**, 861.
30 C. E. Laplaza, M. J. A. Johnson, J. C. Peters, A. L. Odom, E. Kim, C. C. Cummins, G. N. George and I. J. Pickering, Dinitrogen cleavage by three-coordinate molybdenum(III) complexes: Mechanistic and structural data, *J. Am. Chem. Soc.*, 1996, **118**, 8623.
31 R. Thompson, B. L. Tran, S. Ghosh, C. H. Chen, M. Pink, X. Gao, P. J. Carroll, M. H. Baik and D. J. Mindiola, Addition of Si-H and B-H bonds and redox reactivity involving low-coordinate nitrido-vanadium complexes, *Inorg. Chem.*, 2015, **54**, 3068.
32 L. N. Grant, B. Pinter, T. Kurogi, M. E. Carroll, G. Wu, B. C. Manor, P. J. Carroll and D. J. Mindiola, Molecular titanium nitrides: nucleophiles unleashed, *Chem. Sci.*, 2017, **8**, 1209.
33 D. Martelino, S. Mahato, W. VandeVen, N. M. Hein, R. M. Clarke, G. A. MacNeil, F. Thomas and T. Storr, Chromium Nitride Umpolung Tuned by the Locus of Oxidation, *J. Am. Chem. Soc.*, 2022, **144**, 11594.
34 S. N. Brown, Insertion of a metal nitride into carbon-carbon double bonds, *J. Am. Chem. Soc.*, 1999, **121**, 9752.
35 T. J. Crevier and J. M. Mayer, Direct Attack of Phenyl Anion at an Electrophilic Osmium–Nitrido Ligand, *J. Am. Chem. Soc.*, 1998, **120**, 5595.
36 W.-L. Man, W. W. Y. Lam, H.-K. Kwong, S.-M. Yiu and T.-C. Lau, Ligand-Accelerated Activation of Strong C-H Bonds of Alkanes by a (Salen)ruthenium(VI)–Nitrido Complex, *Angew. Chem., Int. Ed.*, 2012, **51**, 9101.
37 W.-L. Man, T.-M. Tang, T.-W. Wong, T.-C. Lau, S.-M. Peng and W.-T. Wong, Highly Electrophilic (Salen)ruthenium (VI) Nitrido Complexes, *J. Am. Chem. Soc.*, 2004, **126**, 478.
38 E. M. Zolnhofer, M. Käß, M. M. Khusniyarov, F. W. Heinemann, L. Maron, M. van Gastel, E. Bill and K. Meyer, An Intermediate Cobalt(IV) Nitrido Complex and its N-Migratory Insertion Product, *J. Am. Chem. Soc.*, 2014, **136**, 15072.
39 M. G. Scheibel, Y. L. Wu, A. C. Stuckl, L. Krause, E. Carl, D. Stalke, B. de Bruin and S. Schneider, Synthesis and Reactivity of a Transient, Terminal Nitrido Complex of Rhodium, *J. Am. Chem. Soc.*, 2013, **135**, 17719.
40 J. Schoffel, A. Y. Rogachev, S. DeBeer George and P. Burger, Isolation and hydrogenation of a complex with a terminal iridium-nitrido bond, *Angew. Chem., Int. Ed.*, 2009, **48**, 4734.
41 V. Vreeken, M. A. Siegler, B. de Bruin, J. N. Reek, M. Lutz and J. I. van der Vlugt, C-H Activation of Benzene by a Photoactivated Ni(II)(azide): Formation of a Transient Nickel Nitrido Complex, *Angew. Chem., Int. Ed.*, 2015, **54**, 7055.
42 P. Q. Kelly, A. S. Filatov and M. D. Levin, A Synthetic Cycle for Heteroarene Synthesis by Nitride Insertion**, *Angew. Chem., Int. Ed.*, 2022, **61**, e202213041.
43 H. Shi, H. K. Lee, Y. Pan, K.-C. Lau, S.-M. Yiu, W. W. Y. Lam, W.-L. Man and T.-C. Lau, Structure and Reactivity of a Manganese(VI) Nitrido Complex Bearing a Tetraamido Macrocyclic Ligand, *J. Am. Chem. Soc.*, 2021, **143**, 15863.
44 F. S. Schendzielorz, M. Finger, C. Volkmann, C. Würtele and S. Schneider, A Terminal Osmium(IV) Nitride: Ammonia Formation and Ambiphilic Reactivity, *Angew. Chem., Int. Ed.*, 2016, **55**, 11417.
45 T. J. Crevier, B. K. Bennett, J. D. Soper, J. A. Bowman, A. Dehestani, D. A. Hrovat, S. Lovell, W. Kaminsky and J. M. Mayer, C–N Bond Formation on Addition of Aryl Carbanions to the Electrophilic Nitrido Ligand in TpOs(N)Cl2, *J. Am. Chem. Soc.*, 2001, **123**, 1059.

46 C. Schiller, D. Sieh, N. Lindenmaier, M. Stephan, N. Junker, E. Reijerse, A. A. Granovsky and P. Burger, Cleavage of an Aromatic C–C Bond in Ferrocene by Insertion of an Iridium Nitrido Nitrogen Atom, *J. Am. Chem. Soc.*, 2023, **145**, 11392.
47 G. P. Connor, B. Q. Mercado, H. M. C. Lant, J. M. Mayer and P. L. Holland, Chemical Oxidation of a Coordinated PNP-Pincer Ligand Forms Unexpected Re–Nitroxide Complexes with Reversal of Nitride Reactivity, *Inorg. Chem.*, 2019, **58**, 10791.
48 T.-W. Wong, T.-C. Lau and W.-T. Wong, Osmium(vi) Nitrido and Osmium(iv) Phosphoraniminato Complexes Containing Schiff Base Ligands, *Inorg. Chem.*, 1999, **38**, 6181.
49 A. Dehestani, W. Kaminsky and J. M. Mayer, Tuning the Properties of the Osmium Nitrido Group in TpOs(N)X2 by Changing the Ancillary Ligand, *Inorg. Chem.*, 2003, **42**, 605.
50 S. Mahato, W. VandeVen, G. A. MacNeil, J. M. Pulfer and T. Storr, Untangling ancillary ligand donation versus locus of oxidation effects on metal nitride reactivity, *Chem. Sci.*, 2024, **15**, 2211.
51 N. M. Hein, G. A. MacNeil and T. Storr, Elaboration on the Electronics of Salen Manganese Nitrides: Investigations into Alkoxy-Substituted Ligand Scaffolds, *Inorg. Chem.*, 2021, **60**, 16895.
52 R. M. Clarke and T. Storr, Tuning Electronic Structure To Control Manganese Nitride Activation, *J. Am. Chem. Soc.*, 2016, **138**, 15299.
53 F. Thomas, Ligand-centred oxidative chemistry in sterically hindered salen complexes: an interesting case with nickel, *Dalton Trans.*, 2016, **45**, 10866.
54 R. M. Clarke, K. Herasymchuk and T. Storr, Electronic structure elucidation in oxidized metal–salen complexes, *Coord. Chem. Rev.*, 2017, **352**, 67.
55 T. Takeyama and Y. Shimazaki, Diversity of oxidation state in copper complexes with phenolate ligands, *Dalton Trans.*, 2024, **53**, 3911.
56 J. Andrez, V. Guidal, R. Scopelliti, J. Pécaut, S. Gambarelli and M. Mazzanti, Ligand and Metal Based Multielectron Redox Chemistry of Cobalt Supported by Tetradentate Schiff Bases, *J. Am. Chem. Soc.*, 2017, **139**, 8628.
57 M. Kawai, T. Yamaguchi, S. Masaoka, F. Tani, T. Kohzuma, L. Chiang, T. Storr, K. Mieda, T. Ogura, R. K. Szilagyi and Y. Shimazaki, Influence of Ligand Flexibility on the Electronic Structure of Oxidized Ni(iii)-Phenoxide Complexes, *Inorg. Chem.*, 2014, **53**, 10195.
58 A. Awasthi, S. C. Mallojjala, R. Kumar, R. Eerlapally, J. S. Hirschi and A. Draksharapu, Altering the Localization of an Unpaired Spin in a Formal Ni(v) Species, *Chem. – Eur. J.*, 2024, **30**, e202302824.
59 A. Awasthi, I. F. Leach, S. Engbers, R. Kumar, R. Eerlapally, S. Gupta, J. Klein and A. Draksharapu, Formation and Reactivity of a Fleeting Ni(iii) Bisphenoxyl Diradical Species, *Angew. Chem., Int. Ed.*, 2022, **61**, e202211345.
60 M. Keener, M. Peterson, R. Hernández Sánchez, V. F. Oswald, G. Wu and G. Ménard, Towards Catalytic Ammonia Oxidation to Dinitrogen: A Synthetic Cycle by Using a Simple Manganese Complex, *Chem. – Eur. J.*, 2017, **23**, 11479.
61 T. Chantarojsiri, A. H. Reath and J. Y. Yang, Cationic Charges Leading to an Inverse Free-Energy Relationship for N—N Bond Formation by MnVI Nitrides, *Angew. Chem., Int. Ed.*, 2018, **57**, 14037.
62 S. V. Park, A. R. Corcos, A. N. Jambor, T. Yang and J. F. Berry, Formation of the N≡N Triple Bond from Reductive Coupling of a Paramagnetic Diruthenium Nitrido Compound, *J. Am. Chem. Soc.*, 2022, **144**, 3259.
63 C. C. Almquist, T. Rajeshkumar, H. Jayaweera, N. Removski, W. Zhou, B. S. Gelfand, L. Maron and W. E. Piers, Oxidation-induced ambiphilicity triggers N-N bond formation and dinitrogen release in octahedral terminal molybdenum(v) nitrido complexes, *Chem. Sci.*, 2024, **15**, 5152.
64 C. C. Almquist, N. Removski, T. Rajeshkumar, B. S. Gelfand, L. Maron and W. E. Piers, Spontaneous Ammonia Activation Through Coordination-Induced Bond Weakening in Molybdenum Complexes of a Dianionic Pentadentate Ligand Platform, *Angew. Chem., Int. Ed.*, 2022, **61**, e202203576.
65 N. G. Léonard, T. Chantarojsiri, J. W. Ziller and J. Y. Yang, Cationic Effects on the Net Hydrogen Atom Bond Dissociation Free Energy of High-Valent Manganese Imido Complexes, *J. Am. Chem. Soc.*, 2022, **144**, 1503.
66 S. Kim, H. Y. Zhong, Y. Park, F. Loose and P. J. Chirik, Catalytic Hydrogenation of a Manganese(v) Nitride to Ammonia, *J. Am. Chem. Soc.*, 2020, **142**, 9518.
67 F. Loose, D. A. Wang, L. Tian, G. D. Scholes, R. R. Knowles and P. J. Chirik, Evaluation of excited state bond weakening for ammonia synthesis from a manganese nitride: stepwise proton coupled electron transfer is preferred over hydrogen atom transfer, *Chem. Commun.*, 2019, **55**, 5595.
68 D. Wang, F. Loose, P. J. Chirik and R. R. Knowles, N–H Bond Formation in a Manganese(v) Nitride Yields Ammonia by Light-Driven Proton-Coupled Electron Transfer, *J. Am. Chem. Soc.*, 2019, **141**, 4795.
69 H. Toda, K. Kuroki, R. Kanega, S. Kuriyama, K. Nakajima, Y. Himeda, K. Sakata and Y. Nishibayashi, Manganese-Catalyzed Ammonia Oxidation into Dinitrogen under Chemical or Electrochemical Conditions, *ChemPlusChem*, 2021, **86**, 1511.
70 R. Kunert, C. Philouze, O. Jarjayes and F. Thomas, Stable M(ii)-Radicals and Nickel(iii) Complexes of a Bis(phenol) N-Heterocyclic Carbene Chelated to Group 10 Metal Ions, *Inorg. Chem.*, 2019, **58**, 8030.
71 E. Peris, Smart N-Heterocyclic Carbene Ligands in Catalysis, *Chem. Rev.*, 2018, **118**, 9988.
72 P. de Frémont, N. Marion and S. P. Nolan, Carbenes: Synthesis, properties, and organometallic chemistry, *Coord. Chem. Rev.*, 2009, **253**, 862.
73 S. Bellemin-Laponnaz, R. Welter, L. Brelot and S. Dagorne, Synthesis and structure of V(v) and Mn(iii)

NHC complexes supported by a tridentate bis-aryloxide-N-heterocyclic carbene ligand, *J. Organomet. Chem.*, 2009, **694**, 604.

74 J. A. Bellow, S. A. Stoian, J. van Tol, A. Ozarowski, R. L. Lord and S. Groysman, Synthesis and Characterization of a Stable High-Valent Cobalt Carbene Complex, *J. Am. Chem. Soc.*, 2016, **138**, 5531.

75 Z. S. Ghavami, M. R. Anneser, F. Kaiser, P. J. Altmann, B. J. Hofmann, J. F. Schlagintweit, G. Grivani and F. E. Kühn, A bench stable formal Cu(iii) N-heterocyclic carbene accessible from simple copper(ii) acetate, *Chem. Sci.*, 2018, **9**, 8307.

76 R. Kunert, C. Philouze, O. Jarjayes, T. Storr and F. Thomas, Single-Oxidation of Ni(ii) Complexes of Bidentate Fused N-Heterocyclic Carbene–Phenol Conjugates, *Organometallics*, 2023, **42**, 1550.

77 C. Gandara, C. Philouze, O. Jarjayes and F. Thomas, Coordination chemistry of a redox non-innocent NHC bis (phenolate) pincer ligand with nickel(ii), *Inorg. Chim. Acta*, 2018, **482**, 561.

78 H. Kropp, A. E. King, M. M. Khusniyarov, F. W. Heinemann, K. M. Lancaster, S. DeBeer, E. Bill and K. Meyer, Manganese nitride complexes in oxidation states III, IV, and V: synthesis and electronic structure, *J. Am. Chem. Soc.*, 2012, **134**, 15538.

79 S. Li, Z. Wang, T. S. A. Hor and J. Zhao, First crystallographic elucidation of a high-valent molybdenum oxo N-heterocyclic carbene complex [CpMoVIO2(IBz)]2 [Mo6O19], *Dalton Trans.*, 2012, **41**, 1454.

80 G. Ciancaleoni, L. Belpassi and F. Marchetti, Back-Donation in High-Valent d0 Metal Complexes: Does It Exist? The Case of NbV, *Inorg. Chem.*, 2017, **56**, 11266.

81 E. L. Rosen, C. D. Jr. Varnado, A. G. Tennyson, D. M. Khramov, J. W. Kamplain, D. H. Sung, P. T. Cresswell, V. M. Lynch and C. W. Bielawski, Redox-Active N-Heterocyclic Carbenes: Design, Synthesis, and Evaluation of Their Electronic Properties, *Organometallics*, 2009, **28**, 6695.

82 W. I. Dzik, X. Xu, X. P. Zhang, J. N. H. Reek and B. de Bruin, 'Carbene Radicals' in CoII(por)-Catalyzed Olefin Cyclopropanation, *J. Am. Chem. Soc.*, 2010, **132**, 10891.

83 A. G. Tennyson, V. M. Lynch and C. W. Bielawski, Arrested Catalysis: Controlling Kumada Coupling Activity via a Redox-Active N-Heterocyclic Carbene, *J. Am. Chem. Soc.*, 2010, **132**, 9420.

84 W. I. Dzik, X. P. Zhang and B. de Bruin, Redox Noninnocence of Carbene Ligands: Carbene Radicals in (Catalytic) C–C Bond Formation, *Inorg. Chem.*, 2011, **50**, 9896.

85 E. V. Ilyakina, A. I. Poddel'sky, A. V. Piskunov, G. K. Fukin, A. S. Bogomyakov, V. K. Cherkasov and G. A. Abakumov, The interaction of N,N′-bis(2,6-dimethylphenyl)imidazol-2-ylidene with o-benzosemiquinonato zinc(ii) and indium (iii) complexes, *New J. Chem.*, 2012, **36**, 1944.

86 C. Romain, S. Choua, J.-P. Collin, M. Heinrich, C. Bailly, L. Karmazin-Brelot, S. Bellemin-Laponnaz and S. Dagorne, Redox and Luminescent Properties of Robust and Air-Stable N-Heterocyclic Carbene Group 4 Metal Complexes, *Inorg. Chem.*, 2014, **53**, 7371.

87 C. F. Harris, M. B. Bayless, N. P. van Leest, Q. J. Bruch, B. N. Livesay, J. Bacsa, K. I. Hardcastle, M. P. Shores, B. de Bruin and J. D. Soper, Redox-Active Bis(phenolate) N-Heterocyclic Carbene [OCO] Pincer Ligands Support Cobalt Electron Transfer Series Spanning Four Oxidation States, *Inorg. Chem.*, 2017, **56**, 12421.

88 J. Beerhues, M. Neubrand, S. Sobottka, N. I. Neuman, H. Aberhan, S. Chandra and B. Sarkar, Directed Design of a AuI Complex with a Reduced Mesoionic Carbene Radical Ligand: Insights from 1,2,3-Triazolylidene Selenium Adducts and Extensive Electrochemical Investigations, *Chem. – Eur. J.*, 2021, **27**, 6557.

89 G. Meloni, L. Beghetto, M. Baron, A. Biffis, P. Sgarbossa, M. Mba, P. Centomo, L. Orian, C. Graiff and C. Tubaro, Manganese(iii) complexes with tetradentate O^C^C^O ligands: Synthesis, characterization and catalytic studies on the CO2 cycloaddition with epoxides, *Mol. Catal.*, 2023, **538**, 113006.

90 J. DuBois, J. Hong, E. M. Carreira and M. W. Day, Nitrogen transfer from a nitridomanganese(v) complex: Amination of silyl enol ethers, *J. Am. Chem. Soc.*, 1996, **118**, 915.

91 J. Bendix, [Cr(N)Cl4]2-: A Simple Nitrido Complex Synthesized by Nitrogen-Atom Transfer, *J. Am. Chem. Soc.*, 2003, **125**, 13348.

92 T. Birk and J. Bendix, Atom transfer as a preparative tool in coordination chemistry. Synthesis and characterization of Cr(v) nitrido complexes of bidentate ligands, *Inorg. Chem.*, 2003, **42**, 7608.

93 G. Golubkov and Z. Gross, Chromium(v) and Chromium (vi) Nitrido Complexes of Tris(pentafluorophenyl)corrole, *Angew. Chem., Int. Ed.*, 2003, **42**, 4507.

94 G. Golubkov and Z. Gross, Nitrogen atom transfer between manganese complexes of salen, porphyrin, and corrole and characterization of a (nitrido)manganese(vi) corrole, *J. Am. Chem. Soc.*, 2005, **127**, 3258.

95 C. C. Hojilla Atienza, A. C. Bowman, E. Lobkovsky and P. J. Chirik, Photolysis and Thermolysis of Bis(imino)pyridine Cobalt Azides: C–H Activation from Putative Cobalt Nitrido Complexes, *J. Am. Chem. Soc.*, 2010, **132**, 16343.

96 D. M. King, F. Tuna, E. J. McInnes, J. McMaster, W. Lewis, A. J. Blake and S. T. Liddle, Isolation and characterization of a uranium(vi)-nitride triple bond, *Nat. Chem.*, 2013, **5**, 482.

97 B. J. Cook, S. I. Johnson, G. M. Chambers, W. Kaminsky and R. M. Bullock, Triple hydrogen atom abstraction from Mn–NH3 complexes results in cyclophosphazenium cations, *Chem. Commun.*, 2019, **55**, 14058.

98 K. Meyer, J. Bendix, E. Bill, T. Weyhermüller and K. Wieghardt, Molecular and Electronic Structure of Nitridochromium(v) Complexes with Macrocyclic Amine Ligands, *Inorg. Chem.*, 1998, **37**, 5180.

99 J. Bendix, S. R. Wilson and T. Prussak-Wieckowska, The Improved Synthesis of [Cr(N)(salen)].CH_3NO2, *Acta Crystallogr., Sect. C: Cryst. Struct. Commun.*, 1998, **54**, 923.

100 C. J. Cramer, J. R. Gour, A. Kinal, M. Wtoch, P. Piecuch, A. R. M. Shahi and L. Gagliardi, Stereoelectronic effects

on molecular geometries and state-energy splittings of ligated monocopper dioxygen complexes, *J. Phys. Chem. A*, 2008, **112**, 3754.

101 M. Keilwerth, J. Hohenberger, F. W. Heinemann, J. Sutter, A. Scheurer, H. Fang, E. Bill, F. Neese, S. Ye and K. Meyer, A Series of Iron Nitrosyl Complexes {Fe–NO}6–9 and a Fleeting {Fe–NO}10 Intermediate en Route to a Metalacyclic Iron Nitrosoalkane, *J. Am. Chem. Soc.*, 2019, **141**, 17217.

102 F. Weinhold, C. R. Landis and E. D. Glendening, What is NBO analysis and how is it useful? Int, *Rev. Phys. Chem.*, 2016, **35**, 399.

103 F. Weinhold and C. R. Landis, *Discovering Chemistry with Natural Bond Orbitals*, Wiley, Hoboken, NJ, 2012.

104 N. G. Connelly and W. E. Geiger, Chemical Redox Agents for Organometallic Chemistry, *Chem. Rev.*, 1996, **96**, 877.

105 D. M. D'Alessandro and F. R. Keene, Current trends and future challenges in the experimental, theoretical and computational analysis of intervalence charge transfer (IVCT) transitions, *Chem. Soc. Rev.*, 2006, **35**, 424.

106 M. Orio, O. Jarjayes, H. Kanso, C. Philouze, F. Neese and F. Thomas, X-Ray, Structures of Copper(II) and Nickel(II) Radical Salen Complexes: The Preference of Galactose Oxidase for Copper(II), *Angew. Chem., Int. Ed.*, 2010, **49**, 4989.

107 A. Dei, D. Gatteschi, L. Pardi, A. L. Barra and L. C. Brunel, Millimeter band EPR spectra reveal large zero-field splittings in copper(II)—semiquinonato complexes, *Chem. Phys. Lett.*, 1990, **175**, 589.

108 J. DuBois, C. S. Tomooka, J. Hong and E. M. Carreira, Nitridomanganese(V) complexes: Design, preparation, and use as nitrogen atom-transfer reagents, *Acc. Chem. Res.*, 1997, **30**, 364.

109 S.-M. Yiu, W. W. Y. Lam, C.-M. Ho and T.-C. Lau, Facile N···N Coupling of Manganese(V) Imido Species, *J. Am. Chem. Soc.*, 2007, **129**, 803.

110 Y. Murata, F. Cheng, T. Kitagawa and K. Komatsu, Generation of Fullerenyl Cation (EtO)2P+(OH) CH2−C60+from RC60−H and from RC60−C60R (R = CH2P(O)(OEt)2), *J. Am. Chem. Soc.*, 2004, **126**, 8874.

111 S. Stoll and A. Schweiger, EasySpin, a comprehensive software package for spectral simulation and analysis in EPR, *J. Magn, Reson.*, 2006, **178**, 42.

112 I. Noviandri, K. N. Brown, D. S. Fleming, P. T. Gulyas, P. A. Lay, A. F. Masters and L. Phillips, The Decamethylferrocenium/Decamethylferrocene Redox Couple: A Superior Redox Standard to the Ferrocenium/Ferrocene Redox Couple for Studying Solvent Effects on the Thermodynamics of Electron Transfer, *J. Phys. Chem. B*, 1999, **103**, 6713.

113 G. Sheldrick, Crystal structure refinement with SHELXL, *Acta Crystallogr., Sect. C: Struct. Chem.*, 2015, **71**, 3.

114 O. V. Dolomanov, L. J. Bourhis, R. J. Gildea, J. A. K. Howard and H. Puschmann, OLEX2: a complete structure solution, refinement and analysis program, *J. Appl. Crystallogr.*, 2009, **42**, 339.

115 M. J. Frisch, *et al.*, *Gaussian 16*, 2016.

116 L. Goerigk and S. Grimme, Efficient and Accurate Double-Hybrid-Meta-GGA Density Functionals—Evaluation with the Extended GMTKN30 Database for General Main Group Thermochemistry, Kinetics, and Noncovalent Interactions, *J. Chem. Theory Comput.*, 2011, **7**, 291.

117 A. Schäfer, H. Horn and R. Ahlrichs, Fully optimized contracted Gaussian basis sets for atoms Li to Kr, *J. Chem. Phys.*, 1992, 2571.

118 A. Schäfer, C. Huber and R. Ahlrichs, Fully optimized contracted Gaussian basis sets of triple zeta valence quality for atoms Li to Kr, *J. Chem. Phys.*, 1994, **100**, 5829.

119 F. Weinhold and J. E. Carpenter, in *The Structure of Small Molecules and Ions*, ed. R. Naaman and Z. Yager, Springer, 1988, p. 227.

120 J. Tomasi, B. Mennucci and E. Cancès, The IEF version of the PCM solvation method: an overview of a new method addressed to study molecular solutes at the QM ab initio level, *J. Mol. Struct.: THEOCHEM*, 1999, **464**, 211.

